Inorganic Chemistry

Article

pubs.acs.org/IC

Acrylic Acid Derivatives of Group 8 Metal Carbonyls: A Structural and Kinetic Study

Bo Li,[†] Samuel J. Kyran,[†] Andrew D. Yeung,[†] Ashfaq A. Bengali,*[,‡] and Donald J. Darensbourg*[,†]

[†]Department of Chemistry, Texas A&M University, 3255 TAMU, College Station, Texas 77843, United States

[‡]Department of Chemistry, Texas A&M University at Qatar, Doha, Qatar

Supporting Information

ABSTRACT: The synthesis, spectroscopic, and X-ray structural studies of acrylic acid complexes of iron and ruthenium tetracarbonyls are reported. In addition, the deprotonated η^2-olefin bound acrylic acid derivative of iron as well as its alkylated species were fully characterized by X-ray crystallography. Kinetic data were determined for the replacement of acrylic acid, acrylate, and methylacrylate for the group 8 metal carbonyls by triphenylphosphine. These processes were found to be first-order in the concentration of metal complex with the rates for dissociative loss of the olefinic ligands from ruthenium being much faster than their iron analogues. However, the ruthenium derivatives afforded formation of primarily *mono*-phosphine metal tetracarbonyls, whereas the iron complexes led largely to *trans-di*-phosphine tricarbonyls. This difference in behavior was ascribed to a more stable spin crossover species $^3Fe(CO)_4$ which undergoes rapid CO loss to afford the *bis* phosphine derivative. The activation enthalpies for dissociative loss of the deprotonated η^2-bound acrylic acid ligand were found to be larger than their corresponding values in the protonated derivatives. For example, for dissociative loss of the protonated and deprotonated acrylic acid derivatives of iron(0) the $\Delta H^{\ddagger}$ values determined were 28.0 ± 1.2 and 34.1 ± 1.5 kcal·mol^{-1}, respectively. Density functional theory (DFT) computations of the bond dissociation energies (BDEs) in these acrylic acids and closely related complexes were in good agreement with enthalpies of activation for these ligand substitution reactions, supportive of a dissociative mechanism for olefin displacement. Processes related to catalytic production of acrylic acid from CO_2 and ethylene are considered.

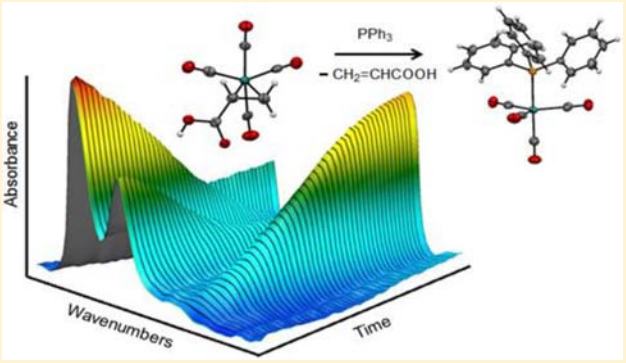

INTRODUCTION

Much effort by researchers worldwide is currently being focused on finding alternative, renewable sources of chemical carbon to replace declining petroleum resources. Utilizing CO_2 for the synthesis of useful organic compounds can be part of a solution to this problem, thereby contributing to a green and sustainable chemical industry.[1] A chemical process under investigation dating back several decades involves the oxidative coupling of CO_2 and ethylene at transition metal centers. This problem was initially addressed by Hoberg in the 1980s using nickel(1,5,9-cyclododecatriene) in the presence of 1,2-*bis*(dicyclohexylphosphino)ethane (dcpe) or 2,2′-bipyridine (bipy).[2] In this manner, ethylene and CO_2 react to provide an oxanickel cyclopentanone which can be decomposed to other organic compounds (Scheme 1). Unfortunately, these processes are stoichiometric in nickel(0) complexes, and catalytic reactions would be highly desirable.

The oxidative coupling of ethylene and CO_2 to afford acrylic acid in the gas phase is slightly endothermic with an enthalpy of reaction of 4.65 kcal/mol (eq 1). This along with a sizable

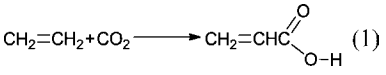

(1)

Scheme 1

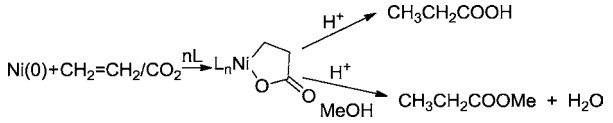

negative entropy of reaction makes the process thermodynamically nonspontaneous at all temperatures. In the presence of hydrogen bonding solvents such as methanol, ΔH of reaction can become exothermic with an estimated value of −4.40 kcal/mol.[3] Similar thermodynamic behavior holds true for the coupling of CO_2 with most saturated and unsaturated hydrocarbons. In the closely related case of the hydrogenation of CO_2 to formic acid, this issue can be overcome in the presence of certain additives, for example, MeOH or Et_3N.[4,5]

Recent kinetic and mechanistic studies of the reaction of (Triphos)Mo$(N_2)_2$(ethylene) with carbon dioxide have shown the oxidative coupling of ethylene and CO_2 to provide the dimeric complex depicted in eq 2.[6] This process is similar to

Received: February 12, 2013
Published: April 24, 2013

   dx.doi.org/10.1021/ic4003737 | *Inorg. Chem.* 2013, 52, 5438−5447

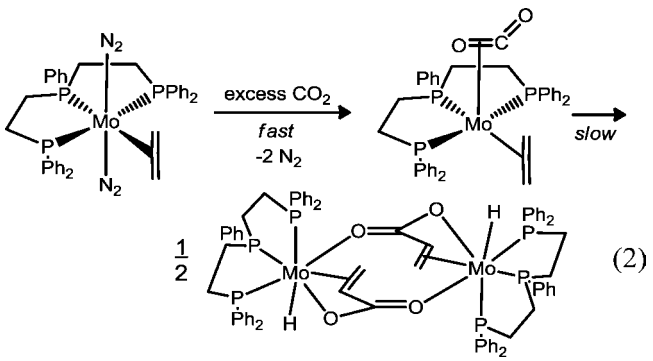

(2)

that previously reported by Carmona and co-workers.[7] Subsequently, Wolfe and Bernskoetter have demonstrated that reaction of the tungsten acrylate complex with an excess of methyl iodide results in the formation of methyl acrylate.[8] An analogous observation has been noted upon reacting the oxanickel cyclopentanone derivative with MeI.[9]

Since ethylene obtained from corn or sugar cane is a renewable resource, preparation of acrylic acid from ethylene and CO_2 would represent an alternative approach to that currently under investigation for the production of bioacrylic acid and its derived poly(acrylic acid). This latter process entails the catalytic dehydration of 3-hydroxypropionic acid (3-HP) produced by microbial conversion of sugar.[10] Recently, Novomer has described a process for the synthesis of polypropiolactone (PPL) from ethylene oxide and CO.[11] Since this stable polymer decomposes cleanly to acrylic acid above 200 °C, it provides a good method for shipping acrylic acid. Presently, we wish to communicate our comprehensive studies of group 8 metal carbonyls with acrylic acid. Specifically, we will describe the binding and removal of the potential product of ethylene/CO_2 coupling, that is, acrylic acid, to zerovalent ruthenium and iron tetracarbonyl derivatives. Our ultimate goal is to find metal complexes which will efficiently couple ethylene and CO_2 in the presence of base to provide an adduct of acrylic acid. Subsequently, the base can be released upon heating and recycled, thereby, leading to a catalytic cycle for the production of this useful carboxylic acid (Scheme 2). The nature of the interaction of the acrylate with the metal center is undefined at this time in the transformations outlined in Scheme 2. This is similar to the mechanism put forth by Buntine and co-workers for the nickel-mediated coupling reaction of CO_2/ethylene to acrylic acid; however, in Scheme 2 triethylamine is used to overcome the unfavorable Gibbs free energy, and ultimately can be recycled upon the addition of thermal energy.[12] Pápai, Aresta, and co-workers have similarly investigated theoretically the mechanism for the coupling of CO_2 and ethylene involving a (bipy)Ni complex.[13]

Scheme 2

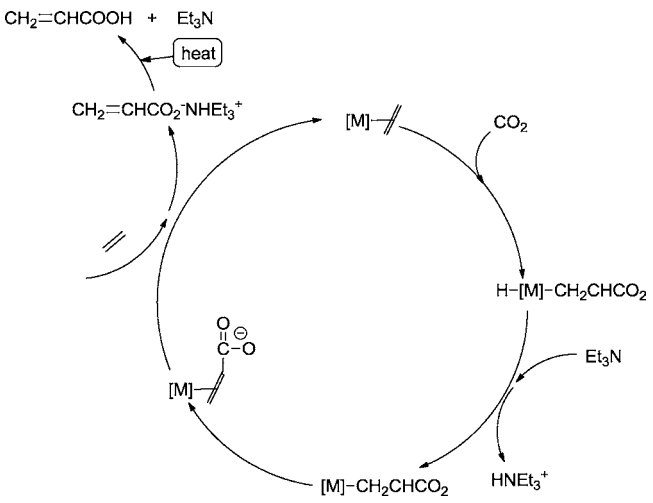

EXPERIMENTAL SECTION

Methods and Materials. All manipulations were carried out using a double manifold Schlenk vacuum line under an argon atmosphere or an argon filled glovebox unless otherwise stated. Reagent grade solvents were purified by an MBraun Manual Solvent Purification System packed with Alcoa F200 activated alumina desiccant. $Fe(CO)_5$ and $Ru_3(CO)_{12}$ were purchased from Strem Chemicals. Acrylic acid, methyl acrylate, piperidine, and PPh_3 were purchased from Sigma-Aldrich. PPh_3 was recrystallized prior to use. $(CH_2$=$CHCOO)Fe(CO)_4^-H_2NC_5H_{10}^+$ was prepared according to literature.[14] $Ru(CO)_4PPh_3$ was prepared by treating a solution of $Ru(CO)_5$ with PPh_3 and stirring overnight.[15] $(CH_2$=$CHCOOMe)Fe(CO)_4$ was prepared in an analogous manner to $(CH_2$=$CHCOOH)Fe(CO)_4$ starting with $Fe(CO)_5$ instead of $Fe_2(CO)_9$.[16,17] Research grade CO and ethylene were obtained from Matheson Tri-Gas. ^{1}H NMR spectra were recorded on a Varian INOVA 300 operating at 299.96 MHz and ^{13}C NMR spectra were recorded on a Varian INOVA 500 operating at 125.59 MHz. The NMR spectra were referenced to residual solvent resonances. Infrared spectra were obtained on a Bruker Tensor 27 FTIR spectrometer. In situ IR monitoring was carried out using a Mettler Toledo iC10 ReactIR with an AgX fiber conduit probe having a SiComp ATR crystal. X-ray crystallography was done on a Bruker-AXS APEXII CCD diffractometer in a nitrogen cold stream maintained at 110 K. Elemental analyses were determined by Atlantic Microlab (Norcross, GA).

Synthesis of $(CH_2$=$CHCOOH)Ru(CO)_4$. A solution of $Ru(CO)_5$ was prepared and used in situ as follows: $Ru_3(CO)_{12}$ (63.9 mg, 0.10 mmol) was dissolved in hexane (100 mL) in a 250 mL Pyrex Schlenk flask. The solution was placed in an ice bath and irradiated using a high-pressure mercury UV lamp (100 W) under a CO atmosphere with slow bubbling for 3 h. During this time the orange solution turned colorless. After removing the excess CO, acrylic acid (69 uL, 1.0 mmol) was added to the above $Ru(CO)_5$ solution and irradiated at room temperature for another 4 h. Removal of solvent under vacuum followed by washing the residue with 5 mL of degassed water and recrystallization from CH_2Cl_2/hexane yielded pale yellow crystals of $(CH_2$=$CHCOOH)Ru(CO)_4$ (36 mg, 42%). IR data in hexane (ν_{CO}): 1675 (m), 2011 (vs), 2039 (s), 2050 (s), 2122 (m). NMR data in $CDCl_3$: ^{1}H δ 2.27 (m, 1 H, CH_2), 2.55 (m, 1 H, CH), 3.04 (m, 1 H, CH_2), 9.20 (s, 1H, COOH); $^{13}C\{^1H\}$ δ 23.5, 34.4, 182.6, 194.4. Anal. Calcd for $C_7H_4O_6Ru$: C, 29.48; H, 1.41 Found: C, 29.66; H, 1.51%.

Synthesis of $(CH_2$=$CHCOOH)Fe(CO)_4$. Similar to the literature method,[17] acrylic acid (0.34 mL, 5.0 mmol) and $Fe(CO)_5$ (10 mL, 74.0 mmol) were added into a 50 mL Pyrex Schlenk flask. The solution was irradiated using a high-pressure mercury UV lamp (100 W) under a CO atmosphere with slow bubbling for 4 h at room temperature. Excess $Fe(CO)_5$ was removed, and the residue was washed with 10 mL of degassed water. Recrystallization from Et_2O/heptane yielded yellow crystals of $(CH_2$=$CHCOOH)Fe(CO)_4$ (0.385 g, 32%). IR data in hexane (ν_{CO}): 1680 (m), 2001 (vs), 2025 (vs), 2038 (s), 2102 (m); ^{13}C NMR could not be collected because of decomposition in solution overnight. Anal. Calcd for $C_7H_4O_6Fe$: C, 35.04; H, 1.68. Found: C, 35.15; H, 1.81%.

Kinetic Measurements. An example of a typical experiment is as follows: $Ru(CO)_4(CH_2$=$CHCOOH)$ (25 mg, 0.087 mmol) and PPh_3 (230 mg, 0.877 mmol) were treated with 5 mL of CH_2Cl_2 under an argon atmosphere in a 3-neck round-bottom flask fitted with the in situ IR probe. Once completely dissolved, the FTIR monitoring was started, and the reaction followed till completion. The reactions were conducted over a 25 K temperature range from 273 to 298 K. In the case of iron tetracarbonyl derivatives, chlorobenzene was used as the

dx.doi.org/10.1021/ic4003737 | Inorg. Chem. 2013, 52, 5438−5447

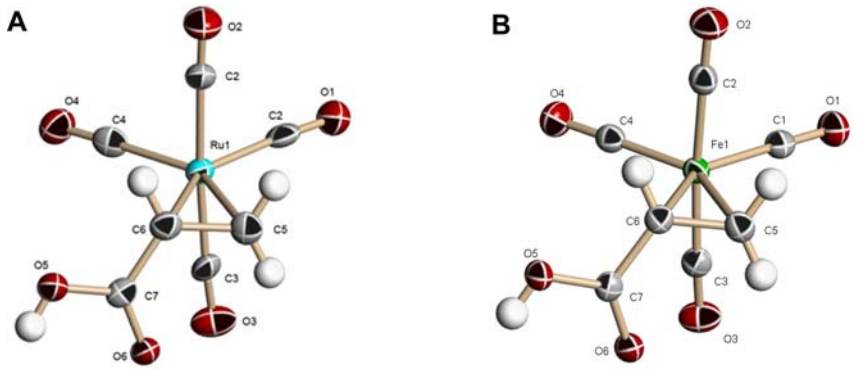

Figure 1. X-ray structures: Thermal ellipsoid representations of **A**, $(CH_2{=}CHCOOH)Ru(CO)_4$, and **B**, $(CH_2{=}CHCOOH)Fe(CO)_4$ with ellipsoids at 50% probability surfaces.

solvent, and the reactions were conducted over a 20 K temperature range from 323 to 343 K.

Computational Methods. All calculations were performed with the Gaussian 09 suite of programs.[18] Geometry optimizations for $Ru(CO)_4$(olefin) complexes were performed using the B3LYP,[19−21] BP86,[19,22] M06,[23] mPWPW91,[24−26] and ωB97X-D[27] functionals. The Pople-style, all-electron 6-311++G(d,p) basis set[28,29] was used for all nonmetal atoms, and the SDD basis set[30−32] and Effective Core Potential (ECP) were used for iron and ruthenium atoms. Local minima were confirmed by their vibrational frequencies (no imaginary vibrational modes). The ωB97X-D functional was found to give the best results in comparison with Poë's data,[33] so it was used for all further calculations.

RESULTS AND DISCUSSION

The synthesis of (acrylic acid)$Fe(CO)_4$ was achieved by photolysis of $Fe(CO)_5$ with acrylic acid at ambient temperature in a modified procedure to that previously published.[17] X-ray quality yellow crystals of this iron derivative were obtained from diethyl ether/heptane. Alternatively, the ruthenium analogue was synthesized in a manner similar to that described by Poë and co-workers.[34] In this instance, it was necessary to first prepare $Ru(CO)_5$ in situ by UV irradiation of $Ru_3(CO)_{12}$ in the presence of CO. Upon removal of excess CO, acrylic acid was added to the solution of $Ru(CO)_5$ and photolysis continued. Following isolation of (acrylic acid)$Ru(CO)_4$, the complex was purified by recrystallization from CH_2Cl_2/hexane to provide pale yellow crystals suitable for X-ray structural analysis. The solid-state structures of these (acrylic acid)$M(CO)_4$ (M = Fe, Ru) complexes display trigonal bipyramidal geometry with the acrylic acid ligand bound by its olefinic function at an equatorial site (Figure 1). A select listings of bond distances and bond angles for these complexes may be found in Table 1. Figure 2 depicts the intermolecular hydrogen-bonding seen between the acrylic acid ligands in the solid-state structures of $(CH_2{=}CHCOOH)Ru(CO)_4$. These complexes' computationally determined geometries are in excellent agreement with the experiment. Both sets of geometric parameters are listed in Table 1.

The infrared spectra of the two group 8 metal derivatives as expected displayed four bands in the ν_{CO} region, along with a carboxyl stretching vibration at ∼1670 cm^{-1}. Figure 3 contains the spectrum of the ruthenium analogue determined in hydrocarbon solvent. At ambient temperature, the four carbonyl ligands are fluxional as indicated by the ^{13}C NMR spectrum of $(CH_2{=}CHCOOH)Ru(CO)_4$, where one broad signal at 194.3 ppm is observed which resolves into four resonances upon lowering the temperature to −40 °C (Figure 4). Intramolecular rearrangement of the carbonyl ligands in olefin tetracarbonyl ruthenium complexes have been reported previously by Grevels, Reuvers, and Takats.[35] Furthermore, Takats and co-workers have determined the energy of activation barriers for this process for several iron derivatives to be 11−14 kcal/mol.[36] It should be noted that the rearrangement of the CO ligands via a Berry process is accompanied by an olefin rotation which likely accounts for the higher barrier for intramolecular rearrangement compared to that seen in $Fe(CO)_5$.[36]

The olefin ligand substitution reactions of (η^2-alkene)$Ru(CO)_4$, where alkene = ethylene and methyl acrylate, with phosphines or phosphites have been shown to proceed via an alkene dissociative process by Chen and Poë.[33] Undoubtedly, the intermediate in this process, $\{Ru(CO)_4\}$, is solvated by the weakly binding solvents used in these processes (Scheme 3). A similar mechanism is anticipated for substitution of acrylic acid

Table 1. Selected Bond Distances (Å) and Angles (deg) for $(CH_2{=}CHCOOH)Ru(CO)_4$ and $(CH_2{=}CHCOOH)Fe(CO)_4$[a,b]

	$(CH_2{=}CHCOOH)Ru(CO)_4$	$(CH_2{=}CHCOOH)Fe(CO)_4$
M(1)−C(1)	1.966 (10); *1.939*	1.811 (3); *1.798*
M(1)−C(2)	1.971 (10); *1.943*	1.825 (3); *1.819*
M(1)−C(3)	1.965 (10); *1.975*	1.825 (3); *1.843*
M(1)−C(4)	1.971 (9); *1.958*	1.809 (3); *1.807*
M(1)−C(5)	2.201 (9); *2.194*	2.088 (3); *2.079*
M(1)−C(6)	2.237 (8); *2.211*	2.101 (2); *2.092*
C(5)−C(6)	1.457 (12); 1.428	1.414 (4); *1.413*
C(6)−C(7)	1.455 (11); *1.477*	1.469 (3); *1.477*
C(7)−O(5)	1.335 (9); *1.348*	1.324 (3); *1.348*
C(7)−O(6)	1.252 (11); *1.209*	1.227 (3); *1.208*
C(1)−M(1)−C(2)	89.8 (4); *90.57*	89.77 (12); *89.74*
C(1)−M(1)−C(3)	88.9 (4); *88.72*	87.47 (12); *88.14*
C(1)−M(1)−C(4)	104.9 (4); *108.68*	109.48 (12); *113.19*
C(1)−M(1)−C(5)	107.9 (3); *107.09*	104.97 (11); *103.02*
C(2)−M(1)−C(3)	175.7 (3); *175.99*	175.77 (12); *177.41*
C(2)−M(1)−C(4)	91.7 (4); *92.32*	91.48 (12); *91.33*
C(2)−M(1)−C(6)	87.2 (3); *85.99*	86.94 (11); *86.49*
C(2)−M(1)−C(5)	90.0 (4); *88.57*	89.19 (11); *90.10*
C(5)−M(1)−C(6)	38.3 (3); *37.82*	39.46 (10); *39.61*
O(5)−C(7)−O(6)	121.5 (7); *121.83*	122.9 (2); *121.96*

[a]Bond distances and angles determined computationally are listed in italics. [b]Data collected at 110 K.

dx.doi.org/10.1021/ic4003737 | *Inorg. Chem.* 2013, 52, 5438−5447

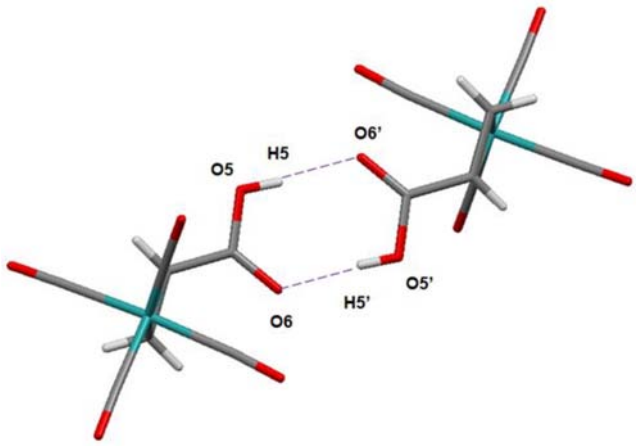

Figure 2. Capped sticks representation of $(CH_2{=}CHCOOH)Ru(CO)_4$ indicating intermolecular hydrogen-bonding, d(O5−O6′) and d(O5′−O6) = 2.656 Å (similarly in the iron derivatives = 2.630 Å).

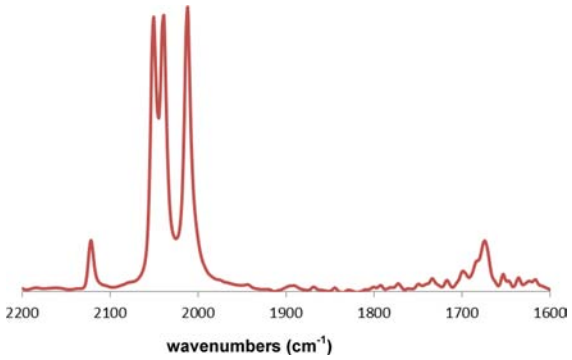

Figure 3. Infrared spectrum of $(CH_2{=}CHCOOH)Ru(CO)_4$ in the carbonyl region.

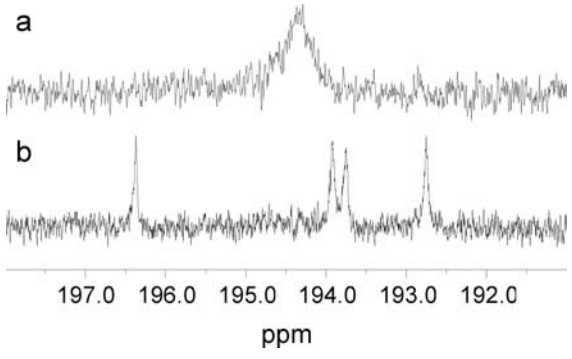

Figure 4. ^{13}C NMR spectra of of (acrylic acid)$Ru(CO)_4$ in $CDCl_3$ at (a) 20 °C (194.3 ppm) and (b) −40 °C (192.7, 193.7, 193.9, and 196.4 ppm).

Scheme 3

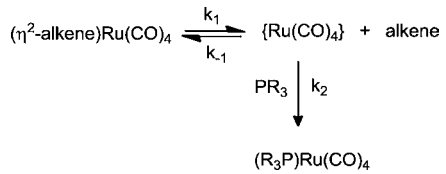

in (acrylic acid)$Ru(CO)_4$ in this study with perhaps minor modifications because of its acidic function. Assuming a steady-state treatment for formation of the intermediate, the dependence of k_{obsd} on the [alkene] and [PR_3] is shown in eq 3. Hence, for the processes carried out in excess [PR_3], k_1 can simply be approximated by k_{obsd}.

$$k_{obsd} = \frac{k_1 k_2 [PR_3]}{k_{-1}[\text{alkene}] + k_2 [PR_3]} \quad (3)$$

The kinetic parameters for the displacement of acrylic acid from (acrylic acid)$Ru(CO)_4$ with triphenylphosphine were determined using in situ infrared monitoring of the ligand substitution process with an iC10 ReactIR instrument. Table 2 contains the ν_{CO} frequencies of the relevant complexes investigated in this study. Figure 5 contains a reaction profile illustrating the disappearance of the parent complex with the concomitant appearance of the mono- and disubstituted triphenylphosphine derivatives in CH_2Cl_2. The temperature dependent rate constants for the substitution of acrylic acid in an equatorial site in (acrylic acid)$Ru(CO)_4$ with triphenylphosphine in an axial site in $(Ph_3P)Ru(CO)_4$ (see X-ray structure in Figure 6) are listed in Table 3 for reactions carried out in 10-fold excess of phosphine. In an accompanying, less productive pathway, a small but significant quantity of *trans*-$(Ph_3P)_2Ru(CO)_3$ was afforded during the substitution process.[37] The extent of CO substitution appears to be slightly dependent on the amount of excess [PPh_3] utilized, as well as the reaction temperatures. See, for example, Figure 7 where the excess [PPh_3] was increased from 10-fold to 30-fold with the %*trans*-$(Ph_3P)_2Ru(CO)_3$ increasing from 17.2% to 24.4%. The negligible change in k_{obsd} upon a 3-fold increase in [PPh_3] is further evidence of the reaction occurring under conditions where $k_{obsd} \approx k_1$.

The slight inhibition noted during the onset of the olefin substitution process (see Figure 5) is thought to be due to adduct formation in the form of hydrogen-bonding between the phosphine ligand and the carboxylic acid functional group (Scheme 4). Indeed, there is a small red shift observed in the ν_{CO} frequencies upon the addition of PPh_3 to a solution of the ruthenium acrylic acid complex, consistent with partial proton abstraction. This red shift is more discernible (10−15 cm^{-1}, see Table 2) for the iron analogue (vide infra). On the other hand, as noted in Table 2, deprotonation of the (acrylic acid)$Ru(CO)_4$ complex with 1 equiv of piperidine results in a red shift of the ν_{CO} bonds of 15−20 cm^{-1}. This in turn leads to a significantly enhanced rate of olefin loss concomitantly without the inhibition step (see Figure 8 and Table 4). As previously

Table 2. Positions of CO Stretching Frequencies for the Relevant Ru and Fe Complexes[a]

complex	ν_{co} (cm^{-1})
$Ru(CO)_4(CH_2{=}CHCOOH)$	2011, 2039, 2050, 2122
$Ru(CO)_4(CH_2{=}CHCOO^{-}NH_2C_5H_{10}^{+})$	1987, 2033, 2109
$Ru(CO)_4PPh_3$	1954, 1988, 2060
$Ru(CO)_3(PPh_3)_2$	1904
$Fe(CO)_4(CH_2{=}CHCOOH)$	2001, 2025, 2038, 2102
$Fe(CO)_4(CH_2{=}CHCOO^{-}NH_2C_5H_{10}^{+})$	1975, 2004, 2016, 2085
$Fe(CO)_4(CH_2{=}CHCOOH)\cdot PPh_3$	1985, 2011, 2029, 2087
$Fe(CO)_4PPh_3$	1944, 1977, 2052
$Fe(CO)_3(PPh_3)_2$	1894
$Fe(CO)_4(CH_2{=}CHCOOMe)$	1997, 2021, 2034, 2100

[a]All spectra determined in hexane solution.

dx.doi.org/10.1021/ic4003737 | Inorg. Chem. 2013, 52, 5438−5447

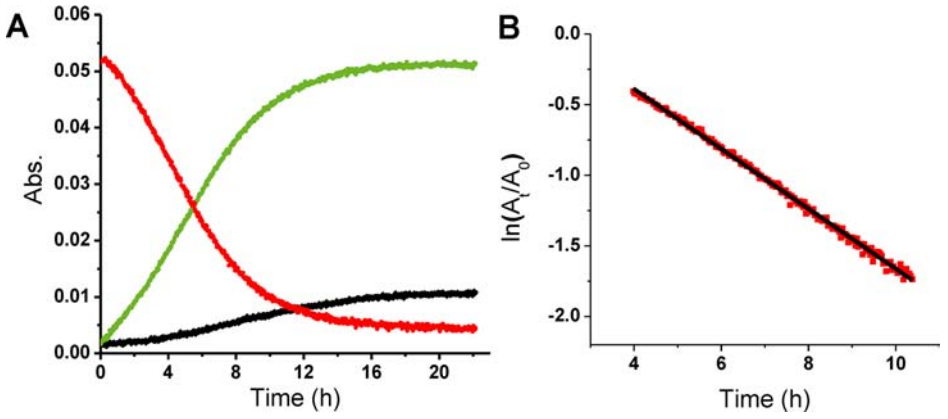

Figure 5. (**A**) Infrared ν_{CO} peak profiles as a function of time for (acrylic acid)$Ru(CO)_4$ (red), $(PPh_3)Ru(CO)_4$ (green), and *trans*-$(PPh_3)_2Ru(CO)_3$ (black) at 283 K in CH_2Cl_2. (**B**) Plot of $\ln(A_t/A_0)$ vs time for disappearance of (acrylic acid)$Ru(CO)_4$, R^2 = 0.997.

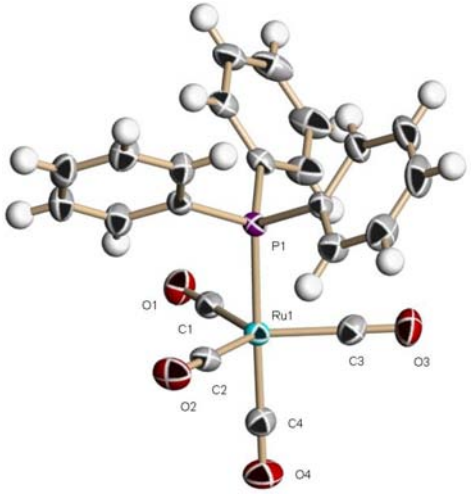

Figure 6. Thermal ellipsoid representation of the X-ray structure of $(Ph_3P)Ru(CO)_4$ with ellipsoids at 50% probability surfaces.

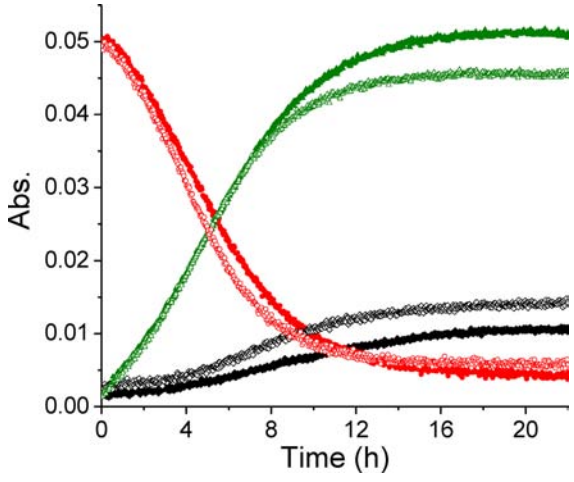

Figure 7. Infrared ν_{CO} profiles for (acrylic acid)$Ru(CO)_4$ disappearance (red) and appearance of $(Ph_3P)Ru(CO)_4$ (green) and *trans*-$(Ph_3P)_2Ru(CO)_3$ (black). Ten-fold excess PPh_3 (solid lines) and 30-fold [PPh_3] (hollow lines) in CH_2Cl_2 at 283 K.

Table 3. Temperature Dependent Rate Constants for the Substitution Reactions of $(CH_2{=}CHCOOH)Ru(CO)_4$ with PPh_3[a]

temperature (K)	$k_{obsd} \times 10^4$ (sec^{-1})	% *trans*-$(Ph_3P)_2Ru(CO)_3$
273	0.102	16.4
283	0.571	17.2
288	1.22	17.9
298	5.09	18.5

[a]Reactions carried out in CH_2Cl_2 with a 10-fold excess of triphenylphosphine.

Scheme 4

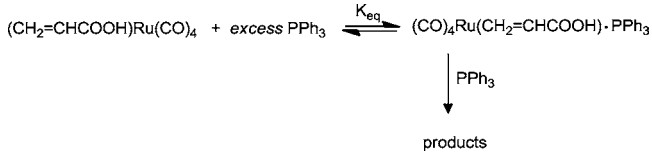

noted, the percentage of disubstitution increases with an increase in temperature. The Eyring plots along with activation parameters for olefin substitution in the presence and absence of piperidine base are depicted in Figure 9.

In an effort to better understand the ligand substitutional behavior of acrylic acid bound to low-valent metal derivatives, we have examined this process in the iron analogue and its ester derivative, $(CH_2{=}CHCOOMe)Fe(CO)_4$. Upon examining the displacement of the acrylic acid ligand in $(CH_2{=}CHCOOH)$-$Fe(CO)_4$ by PPh_3 some striking differences from the course of the ruthenium analogue are noted. As seen in Figure 10, it is apparent that the inhibition step is more pronounced in this instance, and importantly, the product distribution is quite different with the disubstituted phosphine complex being the dominant product. In addition, the ν_{CO} infrared bands for the PPh_3 adduct are red-shifted significantly which allows for monitoring the decrease in both iron carbonyl species with time (Figure 10). Once the equilibrium distribution is established, both forms of the complex must disappear at the same rate. Temperature dependent rate parameters for this process are listed in Table 5, along with the phosphine product distribution.

The addition of 1 equiv of piperidine to $(CH_2{=}$ $CHCOOH)Fe(CO)_4$ leads to the formation of the olefin-bound acrylate iron carbonyl anion and $H_2NC_5H_{10}^+$. X-ray quality crystals of this complex were grown from CH_2Cl_2/hexane, and its structure is illustrated in Figure 11 along with its hydrogen-bonding motif. As noted in Table 2, the ν_{CO} bands in the deprotonated derivative are more red-shifted than in the

dx.doi.org/10.1021/ic4003737 | *Inorg. Chem.* 2013, 52, 5438−5447

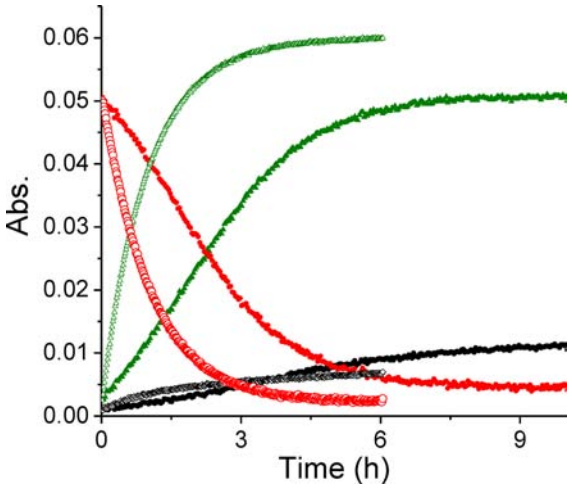

Figure 8. Infrared ν_{CO} peak profiles as a function of time for (acrylic acid)$Ru(CO)_4$ (red), $(PPh_3)Ru(CO)_4$ (green), and *trans*-$(PPh_3)_2Ru(CO)_3$ (black) at 288 K in CH_2Cl_2. Hollow lines with piperidine and solid lines without piperidine.

Table 4. Temperature Dependent Rate Constants for the Substitution Reactions of $(CH_2{=}CHCOOH)Ru(CO)_4$ with PPh_3 in the Presence of Piperidine[a,b]

temperature (K)	$k_{obsd} \times 10^4$ (sec^{-1})	% *trans*-$(Ph_3P)_2Ru(CO)_3$
273	0.152 (*0.102*)	7.75 (*16.4*)
278	0.473	8.40
288	2.20 (*1.22*)	9.61 (*17.9*)
298	9.86 (*5.09*)	11.1 (*18.5*)

[a]Reactions carried out in CH_2Cl_2 with a 10-fold excess of triphenylphosphine and 1 equiv of piperidine. [b]Values in parentheses are from Table 3 for measurements carried out in the absence of piperidine.

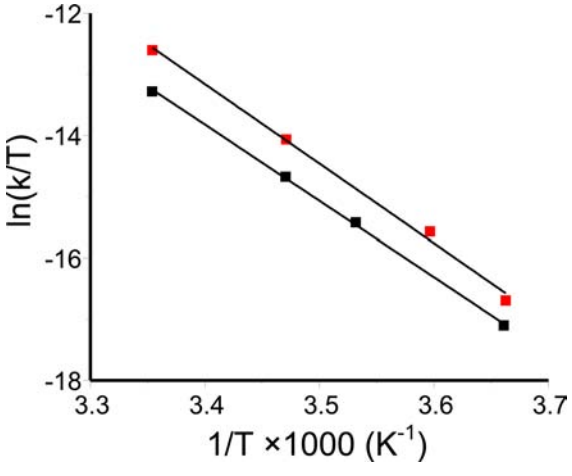

Figure 9. Eyring plots of the substitution reactions of (acrylic acid)$Ru(CO)_4$ with excess PPh_3 in CH_2Cl_2. (red) In the presence of 1 equiv of piperidine (R^2 = 0.994) and $\Delta H^{\ddagger}$ = 26.0 ± 1.1 kcal/mol and $\Delta S^{\ddagger}$ = 14.8 ± 3.9 e.u. (black) in the absence of piperidine (R^2 = 0.999) and $\Delta H^{\ddagger}$ = 24.8 ± 0.4 kcal/mol and $\Delta S^{\ddagger}$ = 9.4 ± 1.4 e.u.

presumably hydrogen bonded adduct with PPh_3. A comparison of the olefin displacement kinetics by PPh_3 from the deprotonated complex vs the protonated version is seen in the reaction profiles shown in Figure 12. As clearly seen, the inhibition step has disappeared in the former case and the % *trans*-$(Ph_3P)_2Fe(CO)_3$ product has decreased. The rate constants for olefin ligand dissociation were slightly smaller than those measured for the process in the absence of piperidine (Table 6), with concomitantly larger values of $\Delta H^{\ddagger}$ and $\Delta G^{\ddagger}$ (see Figure 13).

Further evidence that interaction of the proton in metal bound acrylic acid has influence on the rate of its displacement from the metal center is seen in substitution reactions of the closely related complex, $(CH_2{=}CHCOOMe)Fe(CO)_4$, containing the methyl ester of acrylic acid. As noted in Table 2, the binding abilities of the two olefinic ligands are quite similar, with the ν_{CO} frequencies being within 2−4 cm^{-1} of each other. Furthermore, the solid-state structure and relevant bond distances are correspondingly comparable, Figure 14. Rate constants for the substitution of the methyl ester derivative of acrylic acid are listed in Table 7, with the reaction profiles provided in Figure 15. As is apparent from Figure 15 and Table 7, the substitution reaction is much slower in this instance, and by way of contrast, the monophosphine product is dominant and insensitive to temperature. The activation parameters for the dissociation of the methyl ester of acrylic acid indicated the barrier to be significantly higher in this instance (Table 8).[38]

Early studies by Johnson et al.[39] and Angelici[40] have clearly demonstrated substitution of a CO group from $(Ph_3P)Ru(CO)_4$ or $(Ph_3P)Fe(CO)_4$ with Ph_3P occurs with enthalpies of activation of 30.1 and 42.5 kcal/mol, respectively. Since these values are considerable greater than the corresponding values noted herein for formation of the *bis* phosphine derivatives, an alternative route to these species must be operative. Indeed, observations similar to those noted herein have been reported by Cardaci for several olefinic ligand substitution reactions involving iron tetracarbonyl derivatives.[41] Relevant to these thermal studies are the photosubstitution investigations of iron pentacarbonyl by the groups of Burkey[42] and Harris,[43] respectively. These researchers have shown that CO loss from $^1Fe(CO)_5$ affords the more stable spin crossover species $^3Fe(CO)_4$. This $^3Fe(CO)_4$ species can undergo substitution of a phosphine ligand with spin conservation leading to $^3Fe(CO)_3PPh_3$ which combine with PPh_3 to afford the *bis* phosphine derivative or by a spin crossover process to $^1Fe(CO)_4PPh_3$ (see Scheme 5). The steps following alkene dissociation are essentially barrierless, for example, Harris reported the disubstituted phosphine product formed within 2.5 ns of $^3Fe(CO)_4$ production.[43] Hence, there would not be expected to be much of a temperature or $[PPh_3]$ dependence on the ratio of disubstituted/monosubstituted product as is observed. The rate determining step would be alkene dissociation and the activation enthalpy would parallel the metal-alkene bond dissociation energy (vide infra).

Consistent with this interpretation of the reaction pathway are data obtained in the coordinating solvent acetonitrile as compared to that reported in chlorobenzene. As indicated in Table 9, although the rates of the substitution reactions do not vary significantly in the two solvents, the product distribution does. That is, in the more coordinating solvent CH_3CN, there is an enhancement in the percentage of the disubstituted *trans*-$(PPh_3)_2Fe(CO)_3$ product for the two complexes examined. This is to be expected based on the solvation of the $^3Fe(CO)_4$ intermediate by acetonitrile as observed for methanol by Harris and co-workers.[43]

Theoretical Modeling. In an effort to provide support for the experimental findings, Density Functional Theory (DFT) calculations were performed on several of these complexes.

dx.doi.org/10.1021/ic4003737 | *Inorg. Chem.* 2013, 52, 5438−5447

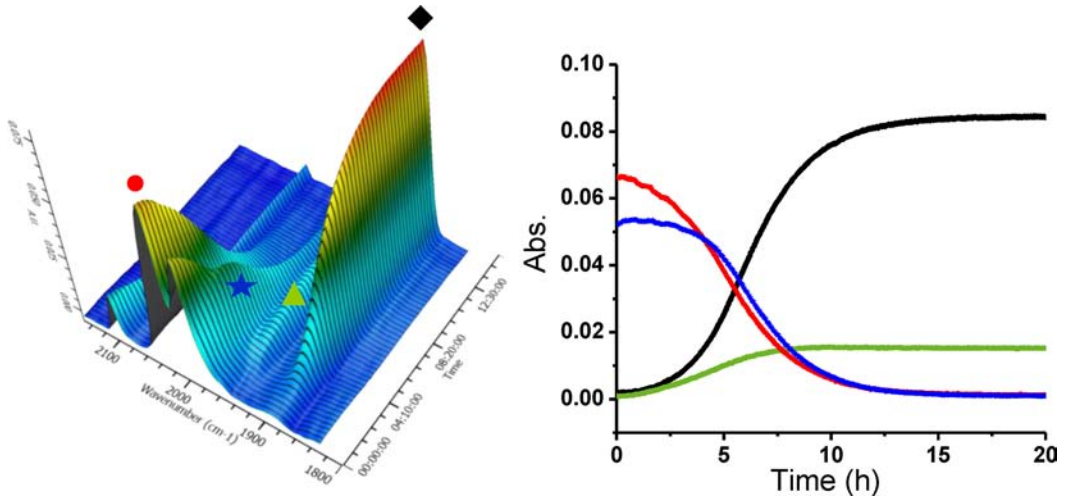

Figure 10. Three-dimensional stack plots (left) for the substitution reaction of $(CH_2{=}CHCOOH)Fe(CO)_4$ with 10 equiv of PPh_3 in chlorobenzene at 328 K. Infrared bands are $(CH_2{=}CHCOOH)Fe(CO)_4$ (red), $PPh_3Fe(CO)_4$ (green), *trans*-$(PPh_3)_2Fe(CO)_3$ (black), and $Fe(CO)_4(CH_2{=}CHCOOH)\cdot PPh_3$ (blue).

Table 5. Temperature Dependent Rate Constants for the Substitution Reactions of $(CH_2{=}CHCOOH)Fe(CO)_4$[a]

temperature (K)	$k_{obsd} \times 10^4$ (sec^{-1})	% *trans*-$(PPh_3)_2Fe(CO)_3$
323	0.667	81.9
328	1.145	84.6
333	2.58	84.8
343	8.57	85.1

[a]Reactions carried out in chlorobenzene with a 10-fold excess of triphenylphosphine.

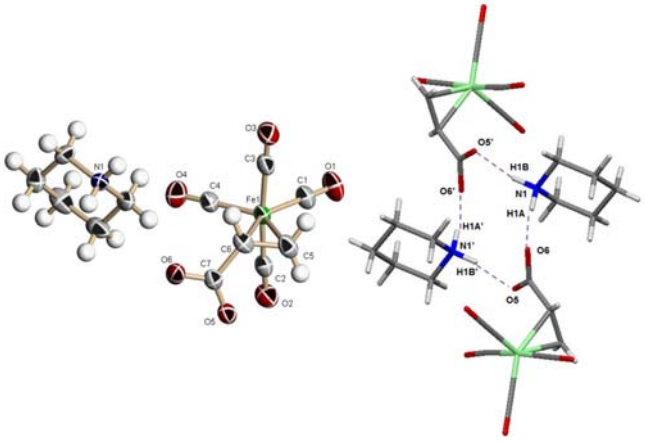

Figure 11. X-ray structure of $(CH_2{=}CHCOO)Fe(CO)_4^-H_2NC_5H_{10}^+$ along with its H-bonding motif with ellipsoids at 50% probability. The Fe−C(5) and Fe−C(6) distances of 2.1049 (19) and 2.1149 (19) Å as well as the C(5)−C(6) distance of 1.410 (3) Å are not statistically different from those found in the parent acrylic acid complex. The *d*(O6−N1) and *d*(O5−N1′) were determined to be 2.710 and 2.703 Å, respectively.

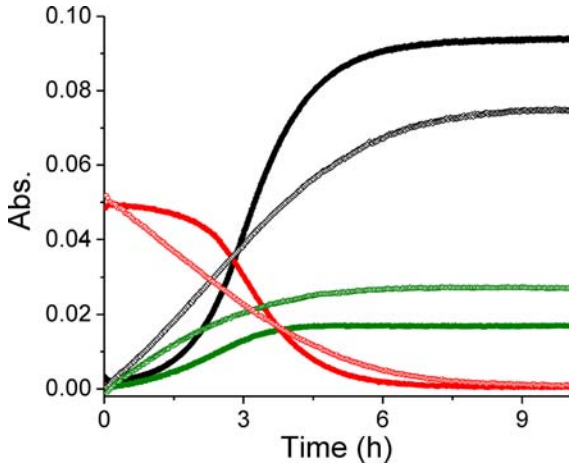

Figure 12. Reaction profiles for $(CH_2{=}CHCOOH)Fe(CO)_4$ + 10 equiv of PPh_3 in chlorobenzene at 333 K, (acrylic acid)$Fe(CO)_4$ (red), $(PPh_3)Fe(CO)_4$ (green), and *trans*-$(PPh_3)_2Fe(CO)_3$ (black). Solid line in absence of piperidine, and hollow line in presence of 1 equiv of piperidine.

Table 6. Temperature Dependent Rate Constants for the Substitution Reactions of $(CH_2{=}CHCOOH)Fe(CO)_4$ with PPh_3 in the Presence of Piperidine[a]

temperature (K)	$k_{obsd} \times 10^4$ (sec^{-1})	% *trans*-$(PPh_3)_2Fe(CO)_3$
323	0.243	72.2
328	0.608	73.0
333	1.47	72.2
343	5.72	71.4

[a]Reactions carried out in CH_2Cl_2 with a 10-fold excess of triphenylphosphine and 1 equiv of piperidine.

Specifically, bond dissociation energies (BDEs) for the olefin-metal bond were calculated for comparison with the experimental activation enthalpies to better assess the ligand substitution pathway. The olefin-metal bond dissociation energy was treated as the energy required for $M(CO)_4L$ to yield two isolated fragments, $M(CO)_4$ and L. In this regard, several functionals were tested, and the ωB97X-D functional was found to give trends most consistent with our results and literature data for a series of closely related complexes (Table 10 and Supporting Information).

In the experiment used to determine the Ru-acrylic acid bond dissociation energy, triphenylphosphine is used to trap the ruthenium tetracarbonyl fragment: $Ru(CO)_4 + PPh_3 \rightarrow Ru(CO)_4PPh_3$. Unfortunately, triphenylphosphine behaves as a Brønsted base, and it is believed to partially afford a polar

dx.doi.org/10.1021/ic4003737 | *Inorg. Chem.* 2013, 52, 5438−5447

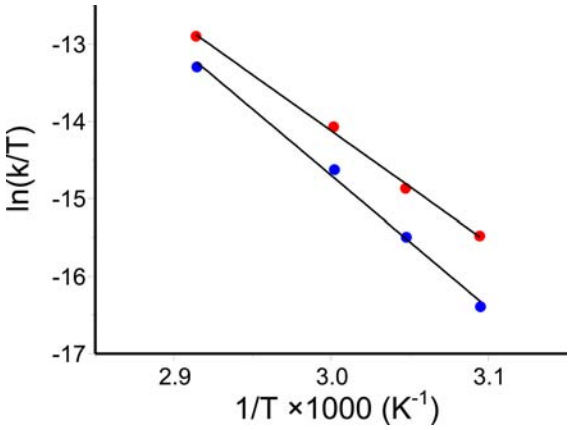

Figure 13. Eyring plots of the substitution reactions of (acrylic acid)$Fe(CO)_4$ with excess PPh_3 in chlorobenzene. (blue) In the presence of 1 equiv of piperidine (R^2 = 0.994) and $\Delta H^{\ddagger}$ = 34.1 ± 1.5 kcal/mol and $\Delta S^{\ddagger}$ = 25.7 ± 4.5 e.u. (red) in the absence of piperidine (R^2 = 0.996) and $\Delta H^{\ddagger}$ = 28.0 ± 1.2 kcal/mol and $\Delta S^{\ddagger}$ = 8.8 ± 3.7 e.u.

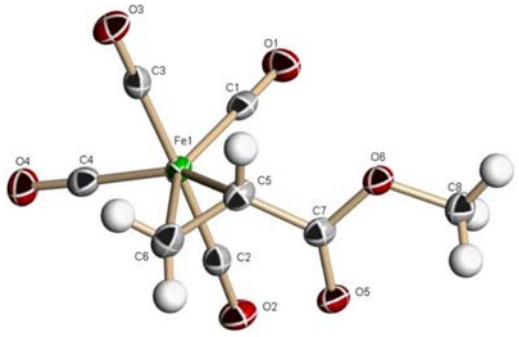

Figure 14. X-ray structure of $(CH_2{=}CHCOOMe)Fe(CO)_4$. The Fe−C(5) and Fe−C(6) distances of 2.108 (2) and 2.101 (2) Å are not statistically different from those found for the acrylic acid and acrylate derivatives.

Table 7. Temperature Dependent Rate Constants for the Substitution Reactions of $(CH_2{=}CHCOOMe)Fe(CO)_4$ with PPh_3[a]

temperature (K)	$k_{obsd} \times 10^4$ (sec^{-1})[b]	% *trans*-$(Ph_3P)_2Fe(CO)_3$
343	0.394	42
353[c]	1.46 (1.58) 1.43[d] (1.61) 1.23[e] (1.30)	42 (42)
358	2.79	42
363	5.45	41

[a]Reactions carried out in chlorobenzene with a 10-fold excess of triphenylphosphine. [b]Rate constants determined from the disappearance of $(CH_2{=}CHCOOMe)Fe(CO)_4$. [c]Rate constant in parentheses were carried out in the presence of a 30-fold excess of triphenylphosphine. [d]Rate constants determined from the appearance of $PPh_3Fe(CO)_4$. [e]Rate constant determined from the appearance of *trans*-$(PPh_3)_2Fe(CO)_3$.

adduct with the carboxylic acid moiety of $Ru(CO)_4$(acrylic acid) in solution. By increasing the electron density on the acrylic acid ligand (more like its conjugate base), it acts as a poorer π-acid, and is more easily dissociated from ruthenium than for L = methyl acrylate. Such interactions are not accounted for in the computations, possibly explaining the small discrepancy between the computed and the experimental results.

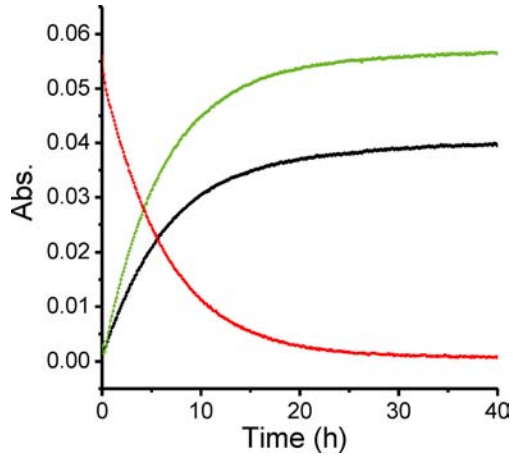

Figure 15. Reaction profiles for $(CH_2{=}CHCOOMe)Fe(CO)_4$ + 10 equiv of PPh_3 in chlorobenzene at 343 K. $(CH_2{=}CHCOOMe)Fe(CO)_4$ (red), $PPh_3Fe(CO)_4$ (green), and *trans*-$(PPh_3)_2Fe(CO)_3$ (black).

Table 8. Summary of Activation Parameters for Olefinic Ligand Dissociation Determined in These Studies.[a]

compound	$\Delta H^{\ddagger}$ (kcal/mol)	$\Delta S^{\ddagger}$ (e.u.)	$\Delta G^{\ddagger}$ (scaled at 298 K)
$(CH_2{=}CHCOOH)Ru(CO)_4$	24.8 ± 0.4	9.4 ± 1.4	22.0
$(CH_2{=}CHCO_2)Ru(CO)_4^{-}H_2NC_5H_{10}^{+}$	26.0 ± 1.1	14.8 ± 3.9	21.6
$(CH_2{=}CHCOOH)Fe(CO)_4$	28.0 ± 1.2	8.8 ± 3.7	25.4
$(CH_2{=}CHCO_2)Fe(CO)_4^{-}H_2NC_5H_{10}^{+}$	34.1 ± 1.5	25.7 ± 4.5	26.4
$(CH_2{=}CHCOOMe)Fe(CO)_4$	31.7 ± 0.5	13.4 ± 1.3	27.7

[a]Ruthenium and iron data determined in CH_2Cl_2 and chlorobenzene, respectively, in the presence of a 10-fold excess of triphenylphosphine.

Compared with ruthenium, the bond dissociation energies for the iron carbonyl complexes were found to be consistently higher by approximately 4 kcal/mol (Table 11). The iron complexes' greater bond dissociation is attributed to iron's greater back-donating ability compared to ruthenium to the olefinic ligand, which results in a stronger iron-olefin bond. Incidentally, compounds of the form $^3M(CO)_4L$ were not found to have stable geometries.

Carbon Dioxide and Ethylene Coupling Reactions. Our preliminary attempts at the oxidative coupling of CO_2 and ethylene involving group 8 metal carbonyls have been unsuccessful. Nevertheless, these studies have suggested future experiments which may be more productive. For example, upon irradiation of $Ru_3(CO)_{12}$ in hexane in the presence of a slow purge of ethylene, complete conversion of $Ru_3(CO)_{12}$ to $(ethylene)_nRu(CO)_{4-n}$ (n = 1 or 2) occurred (eq 4).[45]

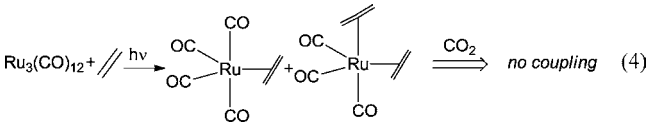

(4)

However, subsequent introduction of CO_2 at atmospheric pressure led to no coupling of CO_2 and ethylene in the presence or absence of triethylamine. A similar observation was

dx.doi.org/10.1021/ic4003737 | Inorg. Chem. 2013, 52, 5438−5447

Scheme 5

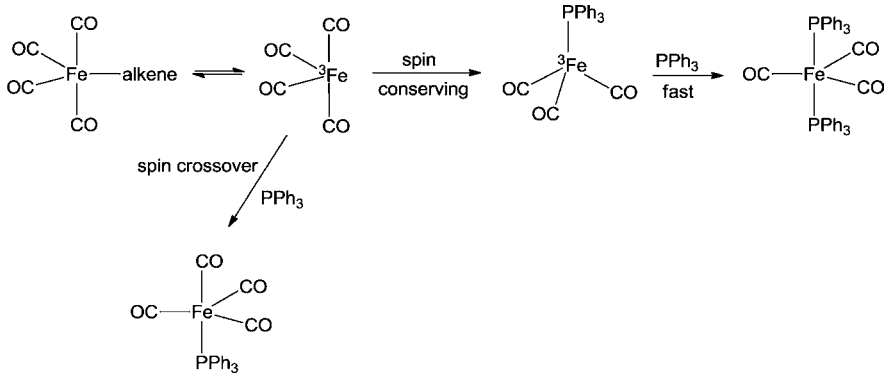

Table 9. Comparison of the Substitution Reaction of (olefin)Fe(CO)$_4$ with PPh$_3$ in Different Solvents[a]

		solvent			
		chlorobenzene		acetonitrile	
olefin	temp. (K)	$k_{obsd} \times 10^4$ (sec^{-1})	% *bis* phosphine	$k_{obsd} \times 10^4$ (sec^{-1})	% *bis* phosphine
CH$_2$=CHCOOH) plus 1 equiv piperidine	333	1.47	72	2.29	100
CH$_2$=CHCOOMe	343	0.394	42	0.174	58

[a]Reactions carried out in 10-fold excess of triphenylphosphine.

Table 10. Calculated Enthalpies (kcal/mol) of the Reaction Ru(CO)$_4$L → Ru(CO)$_4$ + L, Compared with the Experimental Data

	L			
method	C_2H_4	acrylic acid	methyl acrylate	CO
Experimental	24.3[33]	24.8[a]	28.1[33]	27.6[33]
ωB97X-D	27.3	30.1	30.8	29.7

[a]Our result.

Table 11. Enthalpy (kcal/mol) of the Reaction: M(CO)$_4$L → M(CO)$_4$ + L

L	Ru (theor.)	Ru (expt.)	Fe (theor.)	Fe (expt.)
C_2H_4	27.7	24.3[33]	32.3	
acrylic acid	30.5	24.8[a]	34.4	28.0[a]
methyl acrylate	30.4	28.1[33]	34.3	31.7[a]
CO	30.1	27.6[33]	38.8	48[44]

[a]Our results.

noted upon simultaneous introduction of ethylene and CO$_2$ at atmospheric pressure during irradiation of Ru$_3$(CO)$_{12}$. Comparable observations were noted when Ru$_3$(CO)$_{12}$ was replaced with Fe(CO)$_5$. Hence, this would suggest as was observed in the group 6 metal derivatives that a more electron rich metal center is needed to promote the oxidative coupling process.[6,7] Since chelating electron rich diphosphine ligands readily afford ax-eq. substituted (diphosphine)Ru(CO)$_3$ derivatives, these species upon irradiation in the presence of ethylene/CO$_2$ may lead to more productive chemistry.[46,47] Importantly, this approach might lead to an olefin bound intermediate which, as shown herein, could be readily displaced in the presence of olefin to provide a catalytic cycle (Figure 16).

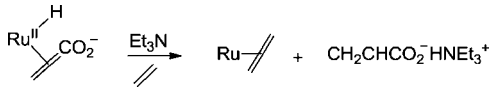

Figure 16. Proposed reaction pathway which accommodates processes described in this report.

CONCLUDING REMARKS

Although these studies have not accomplished our ultimate goal of catalytic oxidative coupling of ethylene and CO$_2$ to afford acrylic acid or its derivatives as mediated by group 8 metal carbonyls, some useful fundamental chemistry closely related to the long-term aims of the study has been forthcoming.[48] That is, the kinetic parameters for the dissociation of the η^2-olefin bound acrylic acid from a conceivable product of ethylene/CO$_2$ coupling, (acrylic acid)M(CO)$_4$ (M = Fe or Ru) and its deprotonated analogue, have been determined. Not unexpectedly, ligand dissociation from the second row transition metal was found to be more facile than from its first row analogue. In addition, although there is little difference in the olefin dissociation kinetic parameters for the protonated or deprotonated forms, the alkylated species is much more kinetically stable toward ligand dissociation. DFT computational studies reveal the activation enthalpies for the metal-olefin dissociation to correlate well with the calculated bond dissociation energies.

ASSOCIATED CONTENT

Supporting Information

CIF files giving X-ray structural data for all complexes studied and a complete listing of all Cartesian coordinates for the modeled complexes. Various functionals tested in theoretical modeling of bond dissociation processes. This material is available free of charge via the Internet at http://pubs.acs.org.

AUTHOR INFORMATION

Corresponding Author

*E-mail: djdarens@mail.chem.tamu.edu (D.J.D.).

Notes

The authors declare no competing financial interest.

ACKNOWLEDGMENTS

This publication was made possible by funding from the Qatar National Research Fund (member of Qatar Foundation), with the synthetic and kinetic studies supported by NPRP Grant 09-157-1-024. The theoretical and crystallographic studies were

funded by the National Science Foundation (CHE 1057743) and the Robert A. Welch Foundation (A-0923). The authors thank Dr. Lisa M. Pérez for valuable discussions, and acknowledge the Laboratory for Molecular Simulation and the Supercomputing Facility at Texas A&M University for providing computing resources.

REFERENCES

(1) Aresta, M. In *Carbon Dioxide as Chemical Feedstock*; Aresta, M., Ed.; Wiley-VCH: Weinheim, Germany, 2010.
(2) (a) Hoberg, H.; Schaefer, D. *J. Organomet. Chem.* **1982**, *236*, C28. (b) Hoberg, H.; Schaefer, D. *J. Organomet. Chem.* **1983**, *251*, C51.
(3) CBS-QB3 calculations performed in the gas phase, and with the use of the SMD solvation model, using methanol as the prototypical solvent.
(4) (a) Darensbourg, D. J.; Ovalles, C. *J. Am. Chem. Soc.* **1984**, *106*, 3750−3754. (b) Darensbourg, D. J.; Ovalles, C.; Pela, M. *J. Am. Chem. Soc.* **1983**, *105*, 5937−5939.
(5) (a) Jessop, P. G.; Hsiao, Y.; Ikariya, T.; Noyori, R. *J. Am. Chem. Soc.* **1996**, *118*, 344−355. (b) Thomas, C. A.; Bonilla, R. J.; Huang, Y.; Jessop, P. G. *Can. J. Chem.* **2001**, *79*, 719−724.
(6) Bernskoetter, W. H.; Tyler, B. T. *Organometallics* **2011**, *30*, 520.
(7) (a) Alvarez, R.; Carmona, E.; Colc-Hamilton, D. J.; Galindo, A.; Gutierrez-Puebla, E.; Monge, A.; Poveda, M. L.; Ruiz, C. *J. Am. Chem. Soc.* **1985**, *107*, 5529. (b) Alvarez, R.; Carmona, E.; Galindo, A.; Gutierrez, E.; Marin, J. M.; Monge, A.; Poveda, M. L.; Ruiz, C.; Savariault, J. M. *Organometallics* **1989**, *8*, 2430. (c) Galindo, A.; Pastor, A.; Perez, P.; Carmona, E. *Organometallics* **1993**, *12*, 4443.
(8) Wolfe, J. M.; Bernskoetter, W. H. *Dalton Trans.* **2012**, *41*, 10763−10768.
(9) (a) Lee, S. Y. T.; Cokoja, M.; Drees, M.; Li, Y.; Mink, J.; Herrmann, W. A.; Kuhn, F. E. *ChemSusChem* **2011**, *4*, 1275. (b) Bruckmeier, C.; Lehenmeier, M. W.; Reichandt, R.; Vagin, S.; Rieger, B. *Organometallics* **2010**, *29*, 2199−2202.
(10) Bomgardner, M. M. *C&E News* **2012**, *90* (35), 8.
(11) Burridge, E. *ICIS Chem. Bus.* **2012**, *22*−*28*, 36.
(12) Graham, D. C.; Mitchell, C.; Bruce, M. I.; Metha, G. F.; Bowie, J. H.; Buntine, M. A. *Organometallics* **2007**, *26*, 6784−6792.
(13) Pápai, I.; Schubert, G.; Mayer, I.; Besenyei, G.; Aresta, M. *Organometallics* **2004**, *23*, 5252−5259.
(14) Darensbourg, D. J.; Tappan, J. E. *J. Organomet. Chem.* **1973**, *54*, C39.
(15) Desrosiers, M. F.; Wink, D. A.; Trautman, R.; Friedman, A. E.; Ford, P. C. *J. Am. Chem. Soc.* **1986**, *108*, 1917.
(16) Weiss, E.; Stark, K.; Lancaster, J. E.; Murdoch, H. D. *Helv. Chim. Acta* **1963**, *46*, 288.
(17) Conder, H. L.; Darensbourg, M. Y. *J. Organomet. Chem.* **1974**, *67*, 93−97.
(18) Frisch, M. J.; Trucks, G. W.; Schlegel, H. B.; Scuseria, G. E.; Robb, M. A.; Cheeseman, J. R.; Scalmani, G.; Barone, V.; Mennucci, B.; Petersson, G. A.; Nakatsuji, H.; Caricato, M.; Li, X.; Hratchian, H. P.; Izmaylov, A. F.; Bloino, J.; Zheng, G.; Sonnenberg, J. L.; Hada, M.; Ehara, M.; Toyota, K.; Fukuda, R.; Hasegawa, J.; Ishida, M.; Nakajima, T.; Honda, Y.; Kitao, O.; Nakai, H.; Vreven, T.; Montgomery, J. A.; Peralta, J. E.; Ogliaro, F.; Bearpark, M.; Heyd, J. J.; Brothers, E.; Kudin, K. N.; Staroverov, V. N.; Kobayashi, R.; Normand, J.; Raghavachari, K.; Rendell, A.; Burant, J. C.; Iyengar, S. S.; Tomasi, J.; Cossi, M.; Rega, N.; Millam, J. M.; Klene, M.; Knox, J. E.; Cross, J. B.; Bakken, V.; Adamo, C.; Jaramillo, J.; Gomperts, R.; Stratmann, R. E.; Yazyev, O.; Austin, A. J.; Cammi, R.; Pomelli, C.; Ochterski, J. W.; Martin, R. L.; Morokuma, K.; Zakrzewski, V. G.; Voth, G. A.; Salvador, P.; Dannenberg, J. J.; Dapprich, S.; Daniels, A. D.; Farkas, Ö.; Foresman, J. B.; Ortiz, J. V.; Cioslowski, J.; Fox, D. J. *Gaussian 09*, Revision B.01; Gaussian Inc.: Wallingford, CT, 2009.
(19) Becke, A. D. *J. Chem. Phys.* **1993**, *98*, 5648−5652.
(20) Lee, C.; Yang, W.; Parr, R. G. *Phys. Rev. B* **1988**, *37*, 785.
(21) Vosko, S. H.; Wilk, L.; Nusair, M. *Can. J. Phys.* **1980**, *58*, 1200.
(22) Perdew, J. P. *Phys. Rev. B* **1986**, *33*, 8822.
(23) Zhao, Y.; Truhlar, D. G. *Theor. Chem. Acc.* **2008**, *120*, 215.
(24) Adamo, C.; Barone, V. *J. Chem. Phys.* **1998**, *108*, 664.
(25) Burke, K.; Perdew, J. P.; Wang, Y. *Derivation of a generalized gradient approximation the PW91 density functional*; Plenum Press: New York, 1998.
(26) Perdew, J. P.; Wang, Y. *Phys. Rev. B* **1992**, *45*, 13244.
(27) Chai, J.-D.; Head-Gordon, M. *Phys. Chem. Chem. Phys.* **2008**, *10*, 6615.
(28) McLean, A. D.; Chandler, G. S. *J. Chem. Phys.* **1980**, *72*, 5639.
(29) Krishnan, R.; Binkley, J. S.; Seeger, R.; Pople, J. A. *J. Chem. Phys.* **1980**, *72*, 650.
(30) Dolg, M.; Wedig, U.; Stoll, H.; Preuss, H. *J. Chem. Phys.* **1987**, *86*, 866.
(31) Igel-Mann, G.; Stoll, H.; Preuss, H. *Mol. Phys.* **1988**, *65*, 1321.
(32) Andrae, D.; Häußermann, U.; Dolg, M.; Stoll, H.; Preuß, H. *Theor. Chim. Acta* **1990**, *77*, 123.
(33) Chen, L.; Poë, A. J. *Inorg. Chim. Acta* **1995**, *240*, 399−404.
(34) (a) Hug, R.; Poë, A. J.; Chawla, S. *Inorg. Chim. Acta* **1980**, *38*, 121−125. (b) Chen, L.; Poë, A. J. *Inorg. Chem.* **1989**, *28*, 3641−3647.
(35) Grevels, F.-W.; Reuvers, J. G. A.; Takats, J. *J. Am. Chem. Soc.* **1981**, *103*, 4069−4073.
(36) Kruczynski, L.; LiShingMan, L. K. K.; Takats, J. *J. Am. Chem. Soc.* **1974**, *96*, 4006−4008.
(37) The *bis* substituted ruthenium product was reported in ref 33 to be obtained in small, unquantifiable amounts.
(38) The $\Delta H^{\ddagger}$ and $\Delta S^{\ddagger}$ for the dissociation of the methyl ester of acrylic acid from $(CH_2{=}CHCOOMe)Ru(CO)_4$ were reported in ref 33 to be 28.1 kcal/mol and 20.5 e.u., respectively.
(39) Johnson, B. F. G.; Lewis, J.; Twigg, M. V. *J. Chem. Soc., Dalton Trans.* **1975**, 1876−1879.
(40) Siefert, E. E.; Angelici, R. J. *J. Organomet. Chem.* **1967**, *8*, 374−376.
(41) (a) Carci, G.; Narciso, V. *J. Chem. Soc., Dalton Trans.* **1972**, 2289−2293. (b) Cardaci, G. *Int. J. Chem. Kinet.* **1973**, *5*, 805−817. (c) Cardaci, G. *J. Organomet. Chem.* **1974**, *76*, 385−391. (d) Cardaci, G. *Inorg. Chem.* **1974**, *13*, 368−371. (e) Cardaci, G. *Inorg. Chem.* **1974**, *13*, 1914−2976.
(42) Nayak, S. K.; Farrell, G. J.; Burkey, T. J. *Inorg. Chem.* **1994**, *33*, 2236−2242.
(43) Snee, P. T.; Payne, C. K.; Mebane, S. D.; Kotz, K. T.; Harris, C. B. *J. Am. Chem. Soc.* **2001**, *123*, 6909−6915.
(44) Smith, G. P.; Laine, R. M. *J. Phys. Chem.* **1981**, *85*, 1620−1622.
(45) Wuu, Y.-M.; Bentsen, J. G.; Brinkley, C. G.; Wrighton, M. S. *Inorg. Chem.* **1987**, *26*, 530−540.
(46) Ferrence, G. M.; Fanwick, P. E.; Kubiak, C. P.; Haines, R. J. *Polyhedron* **1997**, *16*, 1453−1459.
(47) As pointed out by a reviewer, the suggestion that a more electron-rich ruthenium center can aim ethylene/CO_2 coupling may be incorrect based on the limited data available in this area.
(48) Lejkowski, M. L.; Lindner, R.; Kageyama, T.; Bódizs, G. É.; Plessow, P. N.; Müller, I. B.; Schäfer, A.; Rominger, F.; Hoffmann, P.; Futter, C.; Schunk, S. A.; Limbach, M. *Chem.—Eur. J.* **2012**, *18*, 14017−14025.